a large genus of the pea family, common in steppe regions (for example, milk vetch in the United States).
12. "Map of the natural vegetation of Iran" (University of Teheran, Iran, 1970).
13. *Quercus*: oak; *Carpinetum*: hardwood, deciduous trees with beech-like bark; *Fagetum hyrcanum*: a Caspian beech; *Buxetum*: belonging to the boxwood family.
14. N. Golesorkhi, preface to "Explanatory guide for the map of the natural vegetation of Iran" (*12*).
15. N. D. McGlashan, *Gut* **10**, 643 (1969).
16. E. Truog, *Soil Sci. Soc. Amer. Proc.* **11**, 305 (1946).
17. A. S. Prasad, H. H. Sandstead, A. R. Schulert, Abou Shadi el Rooby, *J. Lab. Clin. Med.* **62**, 591 (1963).
18. B. L. Vallee, W. E. C. Wacker, A. F. Bartholomay, F. L. Hoch, *New Engl. J. Med.* **257**, 1055 (1957); B. L. Vallee, W. E. C. Wacker, A. F. Bartholomay, E. D. Robin, *ibid.* **255**, 403 (1956).
19. W. J. Pories, J. H. Henzel, C. G. Rob, W. H. Strain, *Lancet* **1**, 121 (1967).
20. F. Jacobsson, in *Tumours of the Oesophagus*, N. C. Tanner and D. W. Smithers, Eds. (Livingstone, London, 1961), p. 53.
21. E. L. Wynder and J. H. Fryer, *Ann. Intern. Med.* **49**, (No. 5) 1106 (1958).
22. R. J. W. Burrell, W. A. Roach, A. Shadwell, *J. Nat. Cancer Inst.* **36**, 201 (1966).
23. E. F. Rose, *Nat. Cancer Inst. Monogr.* **25**, 83 (1967).
24. A. G. Oettlé, *Cancer Research in Africa*, Raymond Dart lecture No. 3 (Witwatersrand Univ. Press, Johannesburg, 1967).
25. ———, *J. Nat. Cancer Inst.* **33**, 383 (1964).
26. P. N. Sen Gupta, H. Hedayat, H. Hormozdiary, A. Beyzaee, *Report on the Household Food Consumption and Nutrition Survey in the Gorgan Area of the Caspian Sea Region* (Food and Agriculture Organization of the United Nations and Food and Nutrition Institute, Teheran, Report to the Government of Iran No. 9, 1967).
27. I. Martinez, *J. Nat. Cancer Inst.* **42**, 1069 (1969).
28. N. I. Kolycheva, personal communication (1969).
29. M. Segi, M. Kurihara, *Cancer Mortality for Selected Cancer Sites in 24 Countries*, Tohoku University, Ed. (Department of Public Health, School of Medicine, Tohoku University, Sendai, Japan, 1964).
30. *Climatic Atlas of Iran*, plate 1, "Plan organization of Iran," Arid Zone Project No. 550-402 (project executor A. Mostofi, Department of Geography, University of Teheran, 1955).

Ion Microprobe Mass Analyzer

C. A. Andersen and J. R. Hinthorne

The ion microprobe mass analyzer is an instrument that has been developed to provide an in situ mass analysis of a microvolume of the surface of a solid sample. It accomplishes the analysis by bombarding the surface with a high-energy beam of ions, which causes the atoms at the surface to be sputtered away. A fraction of the sputtered particles is electrostatically charged, and these sputtered ions are collected and analyzed according to their mass-to-charge ratio in a mass spectrometer. The instrument complements other microanalytical techniques, such as the electron microprobe x-ray analyzer, by providing information about the concentrations and distribution of the isotopes of the elements in the surface of the solid. The technique permits isotope ratios to be measured, makes it possible to detect the very light elements, and generally extends spatial microanalysis into the range of trace elements. In addition, a highly sensitive analysis can be made of the sample in depth as successive atomic layers of the surface are eroded away by the impinging ion beam.

The general concept of producing a spatially resolved mass analysis of the surface of a solid by bombarding it with a beam of primary ions and analyzing the secondary ions sputtered from the sample was introduced by Castaing and Slodzian (*1*). Their work has resulted in the production of an ion microanalyzer, which has been described by Rouberol *et al.* (*2*) and Socha (*3*). Other sputtering-ion mass spectrometers with varying degrees of microanalytical capability have been described by Barrington *et al.* (*4*), Tamura *et al.* (*5*), and Nishimura and Okano (*6*). An ion microprobe design was proposed by Long (*7*), and a scanning ion microscope based on the design was built and demonstrated by Drummond and Long (*8*). The present article deals with the ion microprobe mass analyzer basically designed by Liebl (*9*). This instrument is parallel in design concept to the electron microprobe x-ray analyzer in that a heavy-ion beam has been substituted for the electron beam and a mass spectrometer for the x-ray spectrometer. This analogy permits a similar microanalytical methodology to be applied in both instruments.

The authors are members of the staff of the Applied Research Laboratories at Hasler Research Center, 95 La Patera Lane, Goleta, California 93017.

Instrumentation

Figure 1 is a schematic diagram of the instrument. The ions used for sample bombardment are generated in a hollow-cathode duoplasmatron ion source that is capable of producing ions of a wide variety of gases, including those of a highly electronegative character. The ions, which can be either positively or negatively charged, are accelerated to energies ranging from 5 to 22.5 kilovolts and passed through the primary mass spectrometer. This spectrometer permits the analyst to select and purify by mass separation a specific chemical species from those produced in the ion source. The purified ion beam is focused to a small probe in an electrostatic lens column consisting of a condenser lens and an objective lens and allowed to impinge on the surface of the sample. The diameter of the ion probe can be varied continuously from about 2 to 500 micrometers. The sample and the point being analyzed can be viewed through an optical microscope while under bombardment.

The sputtered ions are collected and their masses analyzed in a double-focusing mass spectrometer generally similar to the Mattauch-Herzog type, in which the velocity dispersions of the magnetic and electric sectors are matched to permit the acceptance of a wide range of initial energies of the sputtered ions. No entrance slit is used, and the bombarded area is stigmatically focused directly onto the resolving slit. A retrofocal lens is used before the mass spectrometer to increase the solid angle of acceptance of the instrument. Because of the stability of the duoplasmatron ion source and the resulting continuous generation of sputtered sample ions, electrical detection and mass scanning can be used to good advantage.

The ion beams are then detected with a high-gain device of the Daly type (*10*) that permits single-ion counting. Both positive and negative sputtered ions can be detected when the potentials of the conversion electrode and the scintillator are suitably arranged. Sputtered ions from the sample eject secondary electrons at the conversion electrode, and

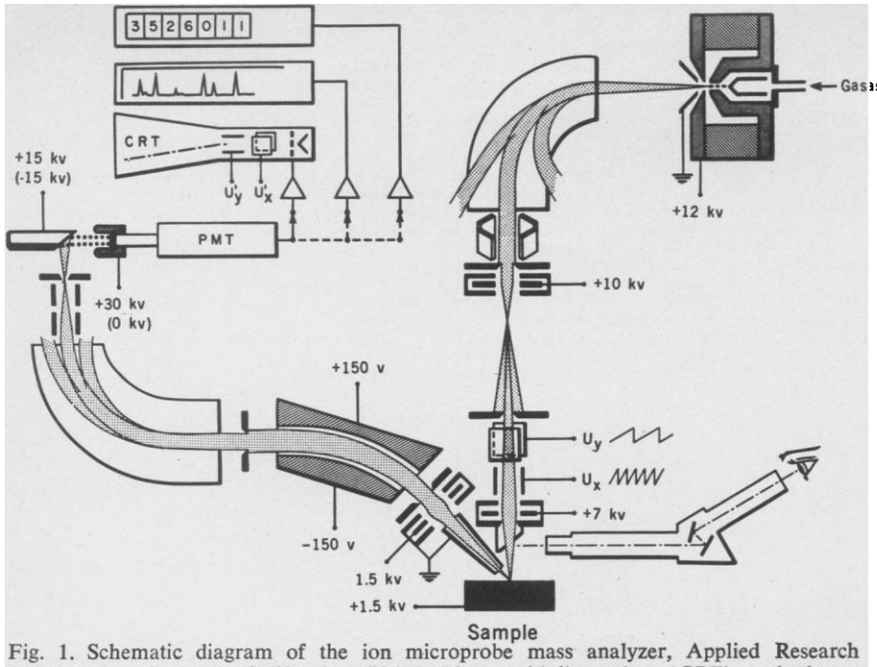

Fig. 1. Schematic diagram of the ion microprobe mass analyzer, Applied Research Laboratories, Sunland, California. (*PMT*) Photomultiplier tube; (*CRT*) cathode-ray tube; (U_x, U_y, U_x', U_y') sweep voltages in x and y directions.

these are accelerated toward the scintillator of a photomultiplier tube, where the light produced by their impact is detected. The resolved ion signals can be read as count rates from scalers, which can accommodate rates in the megacycle range with insignificant dead-time losses, or as direct currents on chart recorders. In the scaling mode no mass-discrimination effects are noted; both heavy and light ions are counted with the same efficiency. To increase the precision of isotope ratio measurements over that obtained by simple mass scanning and counting the ion peaks of interest, the detector assembly has been designed to automatically yield the isotope ratios for isotopes whose mass ranges are within 15 percent of each other. This is accomplished by electrostatically switching the appropriate ion beams in and out of the resolving slit and detector by means of two pairs of electric deflection plates positioned before the slit. The ion beams are switched at a rate of 500 times per second and are recorded separately in the scaling units. A blanking pulse is used between counting intervals to eliminate interference from ion peaks that might fall between the two isotopes of interest. The method has produced, for both metal alloys and bulk insulators, isotope ratios measured with precisions essentially defined by counting statistics down to a practical limit of about 0.1 percent (*11*).

In addition to bombarding a fixed point, the impinging ion beam can be swept over a selected area of the surface of the sample to form a raster by means of the sweeping plates in the primary lens column. The sputtered ions generated by this process are analyzed for mass, and the ion signals can be viewed as a television-like image on a cathode-ray tube. The image gives the two-dimensional distribution of the sputtered element in the selected area. (An example of such a scanning-ion micrograph is given in Fig. 9, which will be discussed in a later section.)

Analytical Method

The analytical method applied with this instrument is based on the observation that the yields of sputtered ions are greatly affected by the surface chemistry of the sample. The sputtered-ion yields of many pure elements have been studied, and the behavior

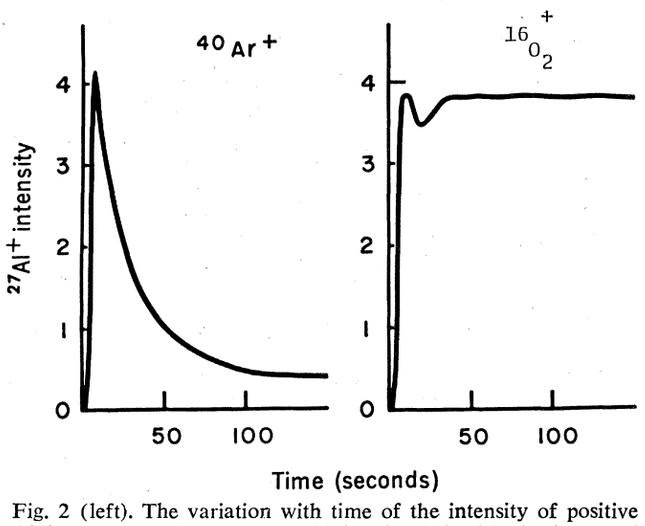

Fig. 2 (left). The variation with time of the intensity of positive Al ions sputtered from pure Al bombarded with Ar ions and with O ions. The sample current is the primary bombarding current measured at the sample. In these experiments, the accelerating potential was 11 kv, the sample current 4×10^{-9} amp, and the probe size 20 μm^2.

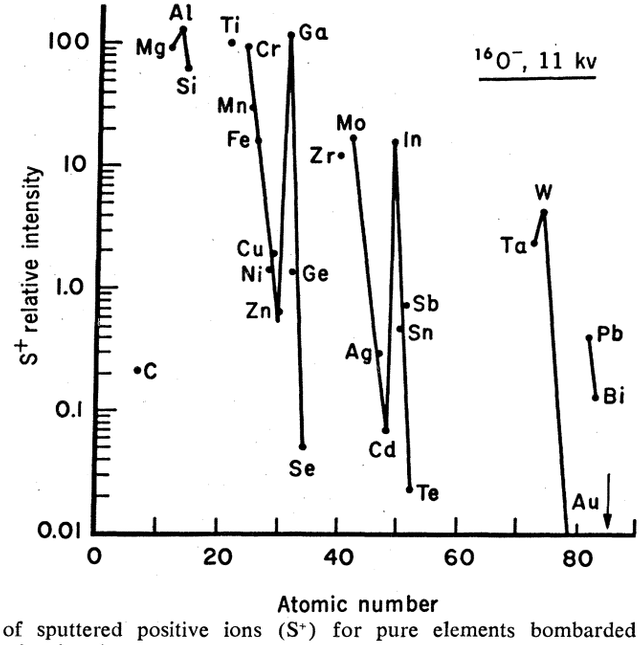

Fig. 3 (right). The relative intensities of sputtered positive ions (S^+) for pure elements bombarded with O ions. The intensities have been corrected for natural isotopic abundances.

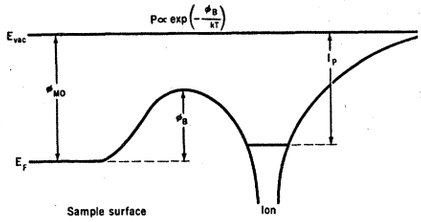

Fig. 4. Probability for neutralization of a positive ion in close proximity to the surface of the solid. The symbol ϕ_B denotes the surface barrier, ϕ_{MO} is the electronic work function of the surface, E_F is the Fermi energy level for electrons in the solid, E_{vac} is the energy level for electrons in a vacuum, and I_p is the ionization energy of the sputtered ion.

illustrated in Fig. 2 (*12*) is typically observed experimentally. When a metal such as aluminum is bombarded with ions of an inert gas such as argon, which has been the common practice, the yield of positive Al ions falls exponentially with time. The ability of the sample to yield positive ions is progressively destroyed by the bombardment. On the basis of the similar behavior of many metals under bombardment by inert gases, it was postulated that the production of sputtered ions is a function of the electronic properties of the surface. The ability to extract positive ions from the sample diminishes as the strongly bonded compounds formed on the surface of the sample through the chemisorption of reactive gases are removed by the eroding action of the bombarding ion beam. In the case of Al it is most likely due to the destruction of the oxidized phase known to exist on its surface. We have shown that the production of positive ions can be maintained at a higher level by controlling the surface chemistry through a proper selection of the species of bombarding ion. Instead of destroying the necessary chemical compounds with an inert gas, it is possible to reconstitute them by bombarding with a reactive gas. The results of bombarding Al with oxygen are also shown in Fig. 2. The yield of Al^+ ions rises to a maximum similar to that observed with Ar bombardment, but instead of decaying exponentially it suffers only a small variation and recovers quickly to maintain a high, stable output of ions. The experimental results indicate that it is possible to manufacture suitable surface compounds at the rate at which they are destroyed by the sputtering process, if the primary ions are a reactive species. This is not a specific effect of oxygen but has been demonstrated to be a general effect of all electronegative gases. Enhanced, stable yields of sputtered positive ions of many pure elements have been produced by bombarding with beams of carbon, nitrogen, oxygen, fluorine, chlorine, and iodine ions (*12*).

Figure 3 (*13*) illustrates the relative sputtered-ion intensities of some pure elements subjected to bombardment by oxygen ions, $^{16}O^-$. The relative intensity for each isotope has been corrected only for its natural abundance. It can be seen that the intensities vary markedly. Those elements that have a high affinity for oxygen (that is, the heat of formation of the metal oxide is large and exothermic) also have the highest sputtered-ion yields. The observed exponential variation in positive-ion emission suggests that the ion yield of a sample is a function of the availability of electrons at the surface.

Electron availability at the surface can be understood, to a first approximation, in terms of the thermionic electron emission of the bombarded surface. In this simple model, illustrated in Fig. 4 (*13*), the probability that an electron will have sufficient energy to be above the surface barrier, ϕ_B, and available for neutralization of the escaping ion is determined by the Fermi distribution of electrons in the material. The probability for neutralization is given by

$$P \propto \exp(-\varphi_B/kT)$$

where ϕ_B is the energy barrier, k is Boltzmann's constant, and T is the absolute temperature of electrons at the surface. At a given temperature corresponding to a given set of bombardment conditions, the number of electrons with sufficient energy to surmount the energy barrier decreases exponentially as the height of the surface barrier increases. The probability of ion neutralization, therefore, decreases as the electronic work function, ϕ_{MO}, of the surface increases. This increase occurs when strongly bonded chemical compounds are formed on the surface because of the chemisorption of electronegative gases. The experimental results indicate that similar types of compounds can be manufactured by bombarding with reactive gases. It should be noted that the ionization potential of the escaping ion, I_p, has no direct influence on the probability of neutralization.

The model proposed for interpreting the emission of sputtered positive ions suggests a method of producing enhanced yields of sputtered negative

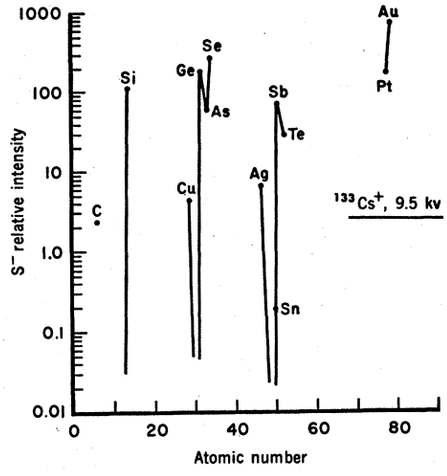

Fig. 5. Relative intensities of sputtered negative ions for elements bombarded with Cs. The intensities have been corrected for natural isotopic abundances.

ions. Positive-ion emission is decreased by electron transfer from the sample surface to the escaping ion. This transfer becomes increasingly prevalent as the energy barrier of the surface decreases. The neutral atoms of many of the most affected elements have large electron affinities. It is possible to take advantage of this fact and produce negative ions by optimizing the conditions for electron transfer from the surface to the sputtered atom. This can be done by reducing the work function of the surface by bombarding it with an electropositive element such as cesium. The relative yields of negative sputtered ions for many elements bombarded with cesium are plotted against atomic number in Fig. 5 (*13*). The yields have been corrected for isotopic

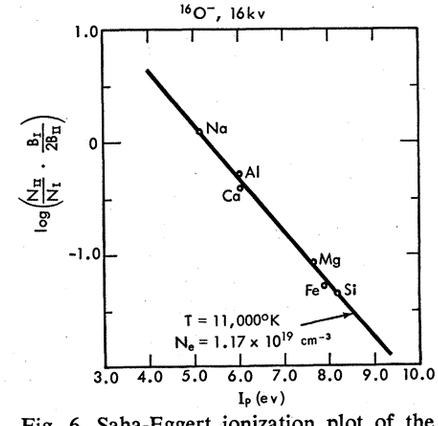

Fig. 6. Saha-Eggert ionization plot of the observed intensities of sputtered ions from a well-characterized mineral standard, clinopyroxene (AC-362-C1). The term ΔE_i, which is a constant for all the elements, is not indicated on the abscissa as it produces only a constant scale change in I_p. In this case ΔE_i is 0.66 electron volt.

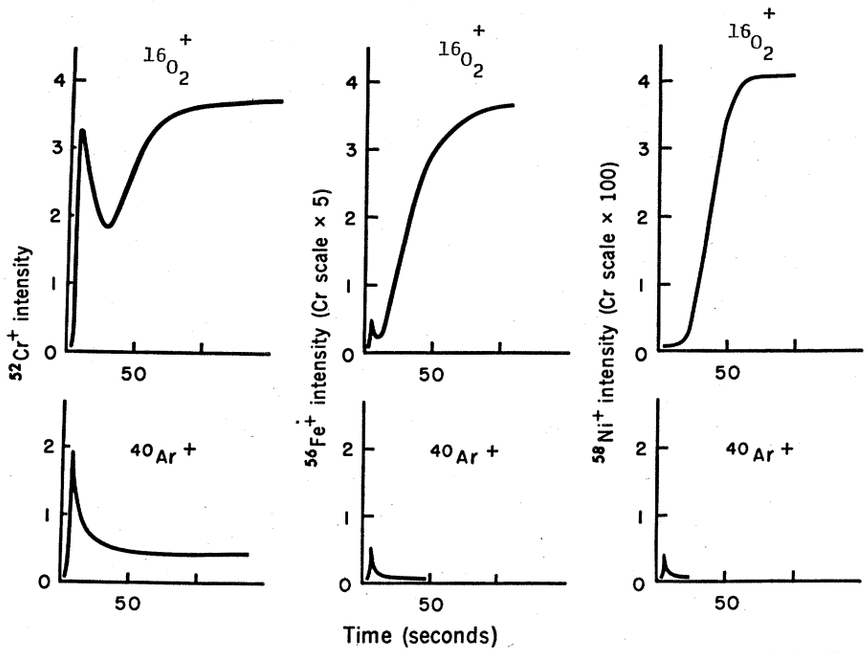

Fig. 7. The variation with time of the intensities of sputtered positive ions of Cr, Fe, and Ni from 304 stainless steel bombarded with oxygen and argon. The sample current is the primary bombarding current measured at the sample. In these experiments, the accelerating potential was 11 kv, the sample current approximately 5×10^{-9} amp, and the probe size approximately 20 μm^2.

abundance and are plotted on the same intensity scale as the yields for positive ions in Fig. 3. It should be noted that the elements shown in Fig. 5 are generally those of low positive-ion yield and high electron affinity. The yield from gold, for example, has increased by six orders of magnitude from its positive-ion yield under oxygen bombardment.

It has been established that sputtered-ion emission from solids can be enhanced and controlled by the proper chemical selection of the primary bombarding ion beam. The model indicates that the attachment of thermionic electrons does not alter the relative ion yields of the elements of a given sample because the common surface barrier of the sample affects all the constituent elements equally. It has also been established that the number of sputtered atoms of a given element is related only to its atomic concentration in the sample (*13*). It appears, therefore, that the only factors that alter the relationship between the relative sputtered-ion yields of the elements and their atomic concentrations in a given sample are those that are related to the excitation and ionization of the sample atoms in the atomic collisions caused by the ion bombardment. In this respect our experiments have indicated that an equilibrium partitioning of excitation energy exists between the atoms in the bombarded region (*14*). Therefore, the energy states of all the particles within the excited volume can be described thermodynamically (*15*) and the ion-to-atom ratio of each element calculated with the Saha-Eggert ionization equation (*16*).

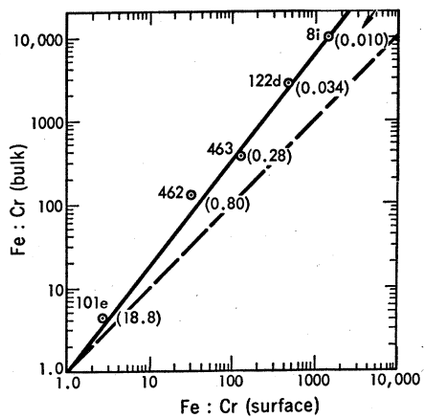

Fig. 8. The measured Fe/Cr ratio of the surface of some Fe alloys as a function of the Fe : Cr ratio of the bulk material, as given by the National Bureau of Standards. The bulk Cr concentration of each sample is given in atomic percent in parentheses. The numbers next to the sample points designate National Bureau of Standards standard reference materials. (8i) Bessemer steel, (122d) cast iron, (463) low alloy steel, (462) low alloy steel, and (101e) 304 stainless steel.

The Saha-Eggert ionization equation gives the ratio of the number of atoms in one charge state to the number of atoms of the same element in the next lower charge state in terms of Boltzmann distribution functions. A practical logarithmic form of the equation is

$$\log \frac{N_{i+1}}{N_i} = 15.38 + \log \frac{2B_{i+1}}{B_i} + 1.5 \log T - \frac{5040\,(I_i - \Delta E_i)}{T} - \log N_e$$

where N_{i+1} and N_i are the numbers of atoms in the two charge states; B_{i+1} and B_i are the partition functions of these charge states; I_i is the ionization potential of the lower charge state; ΔE_i is the depression of the ionization potential due to Coulomb interactions of the charged particles; T is the absolute temperature of the electron, ion, and atom assemblage in degrees Kelvin; and N_e is the number of electrons per cubic centimeter. It can be seen that if the partition functions and ionization potentials are known, the ratio of the number of singly charged ions to the number of neutral atoms of an element is determined by the effective electron temperature and electron density of the assemblage.

Figure 6 (*15*) illustrates the application of this approach to the data for sputtered positive ions from a well-characterized mineral standard. In this case the temperature and electron density of the sputtering assemblage were obtained by solving the Saha-Eggert ionization equation for the best fit of the observed intensities of singly charged ions to the known concentration of the elements in the sample. The fit of the data indicates that the singly charged ions are in thermal equilibrium with the neutral atoms and that the equation can be used to predict their ratio. This is the basis for a quantitative method since the singly charged ions are directly observed in the mass spectrum. Therefore, from the predicted ratio of singly charged to neutral atoms, the total number of atoms of an element present in the sputtering assemblage can be calculated. If all the elements observed in the mass spectrum are treated in this way, the atomic composition of the sample is derived.

The sputtering assemblage is basically a dense plasma of coexisting positive and negative atomic and molecular ions, electrons, and neutral atoms and molecules. Under the present experimental ion-bombardment conditions

most of the particles are neutral atoms and singly charged positive ions. There are, however, for elements of high electron affinity and high oxygen affinity, significant numbers of negative ions and oxide molecules in equilibrium with the positive ions and neutral atoms. The equilibrium concentrations of these species can be calculated with the appropriate Saha equations (*16*) and the intensities of the positive ions corrected for their abundance. All the observed intensities of singly charged positive ions in the mass spectrum are corrected in this way to give the total atomic composition of the sputtering plasma, which is directly related to that of the solid. A computer program entitled Carisma (corrections to Applied Research Laboratories ion-sputtering mass analyzers) has been developed to perform these computations.

The accuracy of the correction procedure is illustrated in Table 1, where analyses for well-characterized, homogeneous mineral standards are given. In each case Carisma was used to find the values of T and N_e, consistent with the observed ion intensities, that gave an absolute atomic composition that best matched the known concentrations of two of the elements in the standard. The observed intensities of all the other elements in the sample were then corrected at the same T and N_e to give the tabulated results. With this method of two internal standards, the concentrations of the major elements are generally within 10 percent of the values determined by wet chemistry. Carisma also contains provisions for using one or no internal standard, but the accuracies of these procedures have not yet been fully evaluated.

Table 2 is a comparison of analyses for major and trace elements in two well-characterized mineral specimens. The comparative analyses for the major and minor elements were performed with an electron microprobe (Applied Research Laboratories model EMX) using well-analyzed mineral standards for calibration (*17*), and those for the trace elements were performed with a spark-source mass spectrometer for solids (AEI Scientific Apparatus, Ltd., model MS-7), with U.S. Geological Survey geochemical rock standards G1 and W1 for calibration (*18*). The ion microprobe analysis was made with the method of two internal standards.

The applicability of the method to the analysis of metals is illustrated in Table 3, where the ion microprobe analyses of National Bureau of Standards steel samples are compared to optical-emission and wet-chemical analyses. The ion microprobe results are based on the method of two internal standards. The lower accuracies here may result from local inhomogeneities in depth as well as inhomogeneities on the surface of the sample.

Applications

Ion-sputtering mass spectrometry has been applied to several problems in the analysis of solids, with various types of instruments. These include studies of oxygen concentrations and concentration gradients and of processes of oxidation in a variety of metals (*19*), a study of some catalytic and corrosion

Table 1. Comparison of ion microprobe and wet-chemical analyses of mineral standards. The numbers AC-362, AC-362-Cl, and AC-362-Or are intralaboratory sample reference numbers.

Element	Plagioclase AC-362		Clinopyroxene AC-362-Cl		Orthopyroxene AC-362-Or	
	Ion	Wet	Ion	Wet	Ion	Wet
Na	3.15	3.14	0.22	0.27	0.054	0.076
Mg			6.39	6.69	9.14	9.03
Al	11.90	11.97	1.07	0.97	0.64	0.66
Si	18.77	18.77	19.56	19.30	19.60	19.60
K	0.16	0.08	0.01	0.02		
Ca	4.30	4.29	8.56	8.54	0.31	0.35
Fe	0.17	0.11	3.98	4.09	9.89	10.0

Table 2. Comparative mineral analyses of Camperdown peridotite. Electron microprobe (EMX) and mass spectrometer (MS-7) analyses were made by the Department of Mineral Sciences of the Smithsonian Institution, Washington, D.C. The analyses labeled IMMA were made with the ion microprobe mass analyzer. The abbreviation n.d. means not determined.

Element	Orthopyroxene			Olivine		
	IMMA	EMX	MS-7	IMMA	EMX	MS-7
	Major elements (atomic percent)					
Si	19.22	19.22		14.21	14.21	
Al	1.42	1.22		n.d.	n.d.	
Mg	17.37	17.58		26.64	25.80	
Fe	1.29	1.72		2.70	2.89	
Ca	0.40	0.31		0.018	0.025	
	Trace elements (atomic parts per million)					
Ti	150		160	77		64
V	45		24	23		4
Cr	1120		1180	195		160
Mn	350		320	340		320
Co	16		19	32		78
Ni	n.d.		240	520		750

Table 3. Comparison of ion microprobe (IMMA) and National Bureau of Standards (NBS) analyses of steels. Concentrations are in atomic percent.

Element	NBS 462 low alloy steel		NBS 101e stainless steel	
	IMMA	NBS	IMMA	NBS
B	0.013	0.0025		
C	1.83	1.83	0.15	0.25
Si	0.60	0.55	0.90	0.84
P	0.012	0.08	0.006	0.044
Ti	0.034	<.042		
V	0.031	0.063	0.058	0.047
Cr	0.95	0.78	19.17	19.04
Mn	1.44	0.94	2.08	1.77
Fe	93.73	94.43	68.73	68.17
Co	0.10	0.10	0.17	0.17
Ni	0.63	0.65	7.28	8.89
Cu	0.20	0.17	0.67	0.31
Zr	0.032	0.038		
Nb	0.042	0.057	0.0088	0.0077
Sn	0.017	0.031	0.068	0.009
Pb	0.0010	0.0016		

Table 4. Abundances of trace elements in Apollo 11 fines material and the crust glass of a breccia. All concentrations are given in atomic parts per million. The abbreviations are M (major element) and n.a. (not analyzed).

Element	Olivine 10085,17-28	Clinopyroxene -26	Plagioclase -25	Ilmenite -28	Crust glass -17
Li	<3	12	17	9	31
B	<12	11	12	<1	26
Na	24	312	3000	18	3800
Mg	M	M	988	18000	M
Al	390	15200	M	1600	M
Si	M	M	M	852	M
P	43	33	32	1.5	130
K	9	14	108	3.5	666
Ca	1230	M	M	<475	M
Ti	475	5200	498	M	M
V	19	69	<0.5	120	45
Cr	680	1340	<2	3300	858
Mn	980	505	42	1600	795
Fe	M	M	1450	M	M
Ni	<45	<1	n.a.	<2	15
Co	17	7	n.a.	11	16
Sr	1.2	4	68	<4	70
Y	0.9	8	<1	5	21
Zr	<1.0	4	<1	36	61
Ba	<0.9	<0.4	<1	n.a.	29
Pb	<1.0	<0.7	<0.5	<1.0	<0.8

processes on metals (*20*), and a study of the chemistry of trace elements in geologic specimens (*21*).

An example of the application of the ion microprobe mass analyzer to surface analysis is the analysis of a polished section of 304 stainless steel (*12*). The intensities of positive sputtered ions of chromium, iron, and nickel were studied as a function of bombardment time and are shown in Fig. 7. As sputtering continues, deeper layers of the sample are exposed and analyzed. The intensity of Cr ions decays at first but then, when oxygen is the bombarding ion, recovers to a high, stable level. According to the proposed model, the original intensity peak indicates that there is a layer of Cr oxide on the surface of stainless steel. This oxide layer is at first destroyed by the eroding action of the sputtering process but is soon reconstituted when oxygen is used in the bombarding beam. As noted earlier, the final level reached in the case of Ar bombardment is a dynamic equilibrium between the cleaning action of the bombarding beam and the recontamination of the surface by the ambient gases in the instrument. A large primary peak is observed in the case of Cr, a much smaller one in the case of Fe, and practically none in the case of Ni. Each curve represents bombardment of a fresh surface spot. This is interpreted to indicate that few Fe atoms and practically no Ni atoms participate in the oxidized phase on the surface of 304 stainless steel.

The Fe/Cr ratio in the surface layers of several steel samples was studied by measuring the intensities of the ion peaks corresponding to the original surface layers in a time study such as those presented in Fig. 7. The measured Fe/Cr ion ratios were quantitatively corrected to yield atom ratios, which are plotted as a function of the Fe/Cr ratio of the bulk material, as given by the National Bureau of Standards, in Fig. 8. A regular dependence of the surface chemistry on the bulk composition is noted, but with the surface layers enriched in Cr over the bulk composition. (As shown in Table 3, the ion microprobe analyses of Fe and Cr in the bulk material of two of these steels, after the surface layers had been sputtered through, compared favorably with those reported by the National Bureau of Standards.) The dashed line indicates a one-to-one correspondence between the Fe/Cr ratios of the bulk and surface layers. The measured ratio deviates from this line in a regular way. As the amount of Cr in the bulk sample decreases, the difference between the surface and bulk Fe/Cr ratio increases, which indicates that a larger relative proportion of the Cr in the bulk of the sample is entering into the surface layers. This apparently indicates that the surface prefers some minimum number of Cr atoms and that these can readily be obtained from the existing reservoir in the bulk of the sample.

The techniques discussed above have been applied to the study of the distribution of trace elements in lunar rocks (*21*). Phenocrysts of the major mineral phases were analyzed in situ in polished thin sections, and quantitative measurements were made of the contents of the major and trace elements. Five thin sections of fragments of four types of Apollo 11 rocks were investigated. The samples were (i) a type A basalt (10085,17-25), (ii) two type B basalts (10085,17-26 and 17-28), (iii) a type C breccia with vein

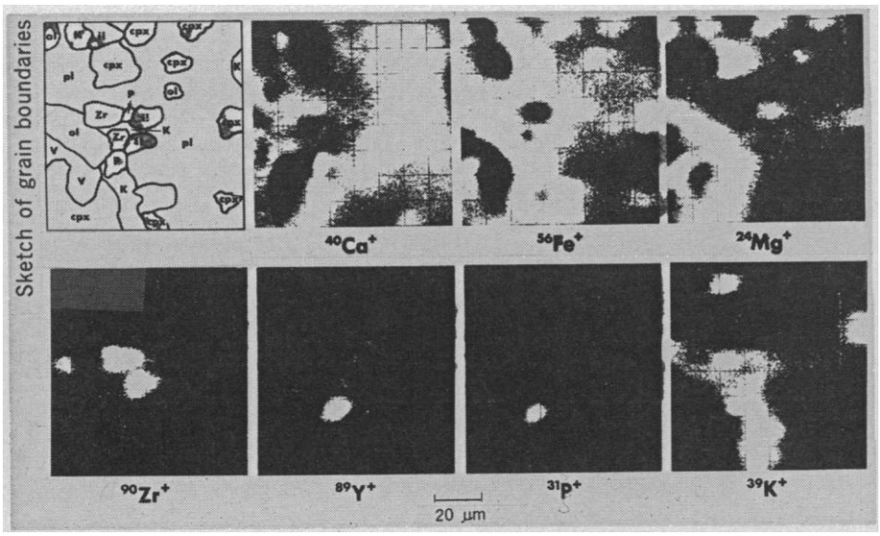

Fig. 9. Scanning-ion micrographs showing the distribution of Ca, Fe, Mg, Zr, Y, P, and K in a type B lunar basalt (10085,17-26). A sketch of the mineral grain boundaries gives the relative positions of the minerals in the scanned area. The abbreviations are *ol* (olivine), *cpx* (clinopyroxene), *pl* (plagioclase), *il* (ilmenite), *Zr* (zirconium oxide), *p* (apatite), *K* (potassium-rich glass), and *V* (void).

glasses and a partial rim of crust glass (10085,17-17), and (iv) an anorthosite-like fragment (10085,7-6).

Table 4 contains typical ion microprobe values of the concentrations of trace elements in all the major mineral phases of Apollo 11 fines material and in the crust glass of a breccia sample that generally represents the bulk chemistry of the rock fines. Several of the elements are more concentrated in the glass than in any of the major mineral phases by about a factor of 2 or more. These are zirconium, yttrium, potassium, phosphorus, barium, lithium, and boron. The data indicate that these elements must be concentrated to a large degree in minor mineral phases not included in this table. A search of the intergranular areas for localized concentrations of these elements was made, and several minor mineral phases were found. The minor phases were tentatively identified as a hafnium-bearing zirconium oxide; a calcium, iron, yttrium, fluorine, rare earth phosphate; a titanium, zirconium, yttrium, rare earth silicate; and a potassium-rich glass phase.

Several of these phases are seen in the scanning-ion micrographs in Fig. 9, which show the distribution of seven elements in a type B lunar basalt (10085,17-26). The distribution of Zr identifies the Zr oxide; that of Y and P the Ca, Fe, Y, F, rare earth phosphate; and that of K, the glass phase. The phases coexist in a matrix of clinopyroxene, plagioclase, ilmenite, and olivine, as shown in a sketch of the mineral grain boundaries determined from the distribution of the major elements. The Ca, rare earth phosphate is probably a fluorapatite, and the Zr oxide is probably a grain of baddeleyite. The potassium-rich glass and the Ti, Zr, Y, rare earth silicate are similar to associations described by Ramdohr and El Goresey (*22*).

Figure 10 shows a partial mass spectrum of the heavy isotopes in the Ti, Zr, Y, rare earth phase. This phase was found as an inclusion in a plagioclase phenocryst in the anorthosite-like fragment 10085,7-6. The mass spectrum shows Ba; abundant rare earths represented by both atomic and molecular monoxide ions; thorium and uranium, represented by molecular monoxide ions; and radiogenic lead. The baddeleyite and apatite phases shown in the micrographs of Fig. 9 also contain abundant Th, U, and radiogenic Pb.

Table 5. Thorium- and uranium-bearing minor mineral phases in Apollo 11 lunar material. The concentration ranges for total Pb are given in atomic parts per million.

Sample number	Phase	Th/U	Total Pb	$^{208}Pb/^{206}Pb$	$^{207}Pb/^{206}Pb$
10085,17-26	Zr oxide	0.49	100–1000	0.13	0.45
10085,7-6	Ti, Zr, Y, rare earth silicate	2.16	1000–2000	0.59	0.40
10085,17-25,-26	Fe, Y, rare earth apatite	5.54	10–50	1.78	0.73

Apparently major portions of the Th, U, and Pb reported on a bulk chemical basis for the Apollo 11 fines material are heterogeneously distributed throughout the rocks in minor mineral phases such as those described here. Finding that Th, U, and their Pb daughter isotopes are concentrated in accessory phases raises the possibility that the separate phases might be radiometrically dated. Such information could be very helpful in understanding the apparently greater age, as determined by $^{207}Pb : ^{206}Pb$ dating (*23*, *24*), of the breccia and fines than of the coexisting, coarser crystalline rock.

Table 5 (*25*) is a summary of the Th/U ratios and the Pb isotopic data for the three minor mineral phases found here. The potassium-rich phase contained no apparent Th, U, or Pb. The isotopic data are preliminary in nature and have an accuracy of only about 10 percent. The Th/U ratio in the three phases varies by more than a factor of 10, and, as expected, the $^{208}Pb/^{206}Pb$ ratio increases linearly with the Th/U ratio. The $^{207}Pb/^{206}Pb$ ratios in the baddeleyite from the type B basalt (10085,17-26) and in the Ti, Zr, Y, rare earth silicate from the anorthosite-like fragment are about the same, within experimental error, and give an apparent age of about 4.1×10^9 years. These ratios correlate with the ratios given by Silver (*23*) for the crystalline rocks. The ratios given in Table 5 for these phases have been corrected for molecular ion interferences, which in both cases are very slight. The apatite phase has a very large $^{207}Pb/^{206}Pb$ ratio, and a large correction for molecular ion interferences was applied in this case. Lead-204 could not be detected in any of the phases, and the common Pb correction was not applied. The $^{207}Pb/^{206}Pb$ ratios reported here, even with relatively large errors, imply that there are individual mineral phases within the fines material that

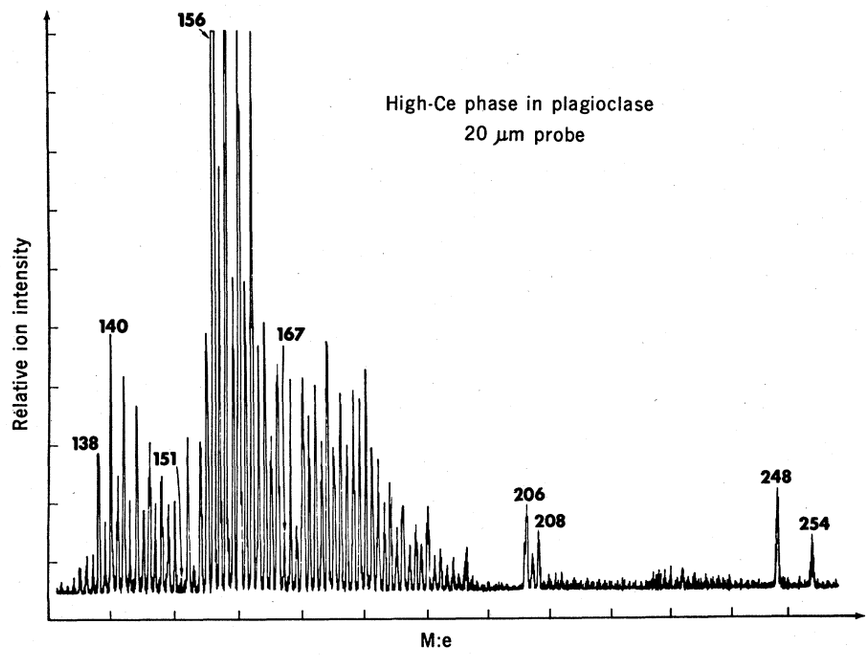

Fig. 10. Partial mass spectrum of the heavy isotopes in the Ti, Zr, Y, and rare earth phase included in a plagioclase in sample (10085, 7-6). The abbreviations are *M/e* (ratio of mass to ion charge), *138* (Ba), *140* (Ce), *151* (Eu), *156* (CeO), *167* (EuO), *206* and *208* (Pb), *248* (ThO), and *254* (UO).

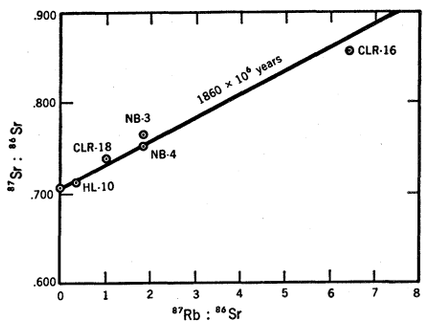

Fig. 11. The ratios $^{87}Rb/^{86}Sr$ and $^{87}Sr/^{86}Sr$ determined by ion microprobe mass analysis for five separate feldspar grains. The initial $^{87}Sr/^{86}Sr$ ratio and the isochron of 1860×10^6 years were determined by Tilton and Sinha (*26*) for bulk specimens, with isotope dilution. The numbers next to the sample points are intralaboratory sample reference numbers.

are of the same approximate age as the coarser crystalline rocks.

The ion microprobe has also been applied, in a preliminary fashion, to the rubidium-strontium dating technique. Potassium feldspar crystals selected from five mineral separates prepared by Tilton and Sinha (*26*) were analyzed with the ion microprobe. Tilton and Sinha determined, by mass spectrometry involving double-filament ionization and isotope dilution, that the ages of all the samples are nearly the same and that they fit an isochron of 1860×10^6 years. The position of this isochron is shown in Fig. 11. Each of the points in the figure represents an ion microprobe analysis of a single 50-μm area on an individual crystal selected from one of the five mineral separates. The relative amounts of ^{87}Sr and ^{87}Rb were determined by measuring the ion intensity of the stable ^{85}Rb isotope and using the known isotopic abundances to predict the intensity of ^{87}Rb. The latter was then subtracted from the intensity observed at mass 87 to yield the ion intensity of ^{87}Sr. The intensities of ^{87}Rb and ^{86}Sr were quantitatively corrected according to the methods proposed in the previous section. The correlation of the ion microprobe results with the independently determined isochron indicates that it may be possible to obtain useful results, for samples on a micrometer scale, from this dating technique.

Conclusion

The quantitative analyses and other applications described in this article indicate a useful future for the ion-microprobe mass analyzer in many areas of the science of solid materials. It should be possible to analyze all the elements quantitatively, but detection sensitivities will vary depending on the matrix, the element, and the polarity of the sputtered ion being studied. Most elements will have optimum yields in the spectrum of positive sputtered ions, and will be detected in concentrations of parts per million in micrometer-sized sampling areas. Electronegative elements will be detected with similar sensitivities in the spectrum of negative sputtered ions, but inert gases, which are ionized with difficulty and have small electron affinities, will be detected with considerably poorer sensitivities. In general, it will be possible to measure isotope ratios without chemical separation of the constituent elements of the sample. The precision of an ion microprobe isotope ratio measurement depends basically on the counting rates involved, and its accuracy can approach its precision if auxiliary standards are used. The isotope ratios of different elements can be compared readily because of the small mass-discrimination effects of the system. Surface layers can be quantitatively analyzed in depth with a resolution of tens of angstroms; hence, it should be possible to study the migration of atoms.

References

1. R. Castaing and G. Slodzian, *J. Microsc. Paris* **1**, 395 (1962).
2. J. M. Rouberol, J. Guernett, P. Deschamps, J. P. Dagnot, J. M. Guyon de la Berge, *Amer. Soc. Test. Mater. Proc.* **68**, 216 (1968).
3. A. J. Socha, *Surface Sci.* **25**, 147 (1971).
4. A. E. Barrington, R. F. S. Herzog, W. P. Poschenrieder, *J. Vac. Sci. Technol.* **3**, 239 (1966).
5. H. Tamura, T. Kondo, H. Doi, I. Omura, S. Taya, in *Recent Developments in Mass Spectrography*, K. Ogata and T. Hayakawa, Eds. (University Park Press, Baltimore, 1970), p. 205.
6. H. Nishimura and J. Okano, *Jap. J. Appl. Phys.* **8**, 1335 (1969).
7. J. V. P. Long, *Brit. J. Appl. Phys.* **16**, 1277 (1965).
8. I. W. Drummond and J. V. P. Long, *Nature* **215**, 952 (1967).
9. H. Liebl, *J. Appl. Phys.* **38**, 5277 (1967); C. F. Robinson, H. J. Liebl, C. A. Andersen, paper presented at the National Conference on Electron Microprobe Analysis 3rd, Chicago, Illinois, 1968.
10. N. R. Daly, *Rev. Sci. Instrum.* **31**, 264 (1960).
11. C. A. Andersen, H. J. Roden, C. F. Robinson, in *Recent Developments in Mass Spectrography*, K. Ogata and T. Hayakawa, Eds. (University Park Press, Baltimore, 1970), p. 215.
12. C. A. Andersen, *Int. J. Mass Spectrom. Ion Phys.* **2**, 61 (1969).
13. ———, *ibid.* **3**, 413 (1970).
14. H. W. Drawin, in *Reactions under Plasma Conditions*, M. Venugopalan, Ed. (Wiley, New York, 1971), vol. 1, p. 53.
15. C. A. Andersen, paper presented at the National Conference on Electron Probe Analysis 6th, Pittsburgh, Pennsylvania, 1971.
16. P. W. J. M. Boumans, *Theory of Spectrochemical Excitation* (Plenum, New York, 1966).
17. J. Nelen, personal communication.
18. B. Mason and A. L. Graham, *Smithson. Contrib. Earth Sci. No. 3* (1970).
19. P. Contamin and G. Slodzian, *C. R. Acad. Sci. Ser. C* **267**, 805 (1968); *Appl. Phys. Lett.* **13**, 416 (1968); V. F. Rybalko, B. Ya. Kolot, Ya. M. Fogel, *Sov. Phys. Tech. Phys.* **14**, 1290 (1970); A. Benninghoven, *Chem. Phys. Lett.* **6**, 626 (1970); C. A. Evans, Jr., *Anal. Chem.* **42**, 1130 (1970).
20. Ya. M. Fogel, *Sov. Phys. Usp.* **10**, 17 (1967).
21. C. A. Andersen, J. R. Hinthorne, K. Fredriksson, in *Proceedings of the Apollo 11 Lunar Science Conference*, A. A. Levinson, Ed. (Pergamon, New York, 1970), vol. 1, p. 159; K. Fredriksson, J. Nelen, A. Noonan, C. A. Andersen, J. R. Hinthorne, in *Proceedings of the Apollo 12 Lunar Science Conference, A. A. Levinson*, Ed. (M.I.T. Press, Cambridge, Mass., in press).
22. P. Ramdohr and A. El Goresey, *Science* **167**, 615 (1970).
23. L. T. Silver, in *Proceedings of the Apollo 11 Lunar Science Conference*, A. A. Levinson, Ed. (Pergamon, New York, 1970), vol. 2, p. 1533.
24. M. Tatsumoto, *ibid.*, p. 1595.
25. K. Fredriksson, J. Nelen, C. A. Andersen, paper presented at the Apollo 12 Lunar Science Conference in Houston, Texas, 1971.
26. G. Tilton and K. Sinha, personal communication.